Bulg. J. Phys. **38** (2011) 72–84

This paper is dedicated to the memory of ***Matey Mateev***

Non-Adiabatic Phonon Dispersion of Graphene

V.N. Popov

Faculty of Physics, University of Sofia, BG-1164 Sofia, Bulgaria

Received *2 February 2011*

Abstract. Recently, failure of the adiabatic approximation has been observed in the charge doping dependence of the Raman spectrum of graphene. The theoretical work has been limited to the phonon dispersion modification in the vicinity of the Brillouin zone center. Here, we present estimation of the non-adiabatic effects on the phonons close to the K point of the Brillouin zone obtained by a perturbation scheme within a non-orthogonal tight-binding model. We show that the explicit account of the dynamic effects change the shape of the Kohn anomaly of the TO phonon branch at the K point. The increase of the charge doping level essentially removes the Kohn anomaly. These results are important for modelling phenomena, in which phonons at the K point are involved, *e.g.*, defect- and second-order Raman scattering.

PACS codes: 63.22.Rc, 73.22.Pr, 78.30.Na

1 Introduction

Graphite has been used in pencils for several hundred years now because thin layers of it are easily exfoliated upon writing on paper. In the atomic energy era graphite is used as neutron moderator. Presently, graphite finds many industrial applications, *e.g.* as electrodes in batteries, reinforcement material, *etc*. The theory predicts that single-layer graphite (graphene) is unstable under ambiant conditions. Recently, high-quality graphene flakes and ribbons have been obtained by mechanical exfoliation [1] and epitaxial growth [2]. Graphene is a zero-gap semiconductor with linear dispersion of the electronic bands close to the Fermi energy at the K and K' points of the hexagonal Brillouin zone. It can easily be doped by electrons or holes [3, 4]. The charge scattering is negligible up to room temperature, which favors ballistic transport [5]. This makes graphene a competitor of silicon in designing nanoelectronic devices.

The Raman spectroscopy ia a straightforward technique to monitor the level of doping of graphene. The Raman spectrum of graphene exhibits a single first-order Raman line, called the G-line and observed at ≈ 1582 cm^{-1}. It is due to the only Raman-active phonon of graphene, the G-mode, of symmetry species E_{2g} with in-plane longitudinal and transverse (LO and TO) polarized components. The Raman measurements of this line upon doping showed strong dependence of the position and linewidth of this line on the Fermi energy shift E_F, which was explained with non-adiabatic effects, arising from strong electron-phonon coupling [3,4,6]. These effects were estimated by use of time-dependent perturbation theory within the density functional theory (DFT) [7].

Large electron-phonon coupling was predicted for the TO-branch phonon at the K point with symmetry $A_1^{'}$ [8, 9] and in-plane breathing-like motion of the hexagons (the $A_1^{'}$-mode) [10]. Therefore, large modification of the TO branch around K point could be expected but has never been explored theoretically before.

Here, we present results of calcualtions of the non-adiabatic phonon dispersion of graphene by use of a perturbative approach [11] within a density-functional-based non-orthogonal tight-binding (NTB) model [12]. We reproduce previous DFT results for the frequency shift and linewidth of the G-mode and report new results for the $A_1^{'}$-mode and for the LO and TO branches in the vicinity of the Γ and K points. The paper is organized as follows. The general theoretical background is given in Section 2, while the details of the calculation of the electronic structure, phonon dispersion, and Raman intensity are provided in Apendix A, B, and C, respectively. The calculated phonon dispersion and linewidth are discussed for the adiabatic approximation (Subsection 3.1), with dynamic corrections (Subsection 3.2), and under charge doping (Subsection 3.3). The paper ends up with conclusions (Section 4).

2 Theoretical Part

The electronic band structure of graphene is calculated within the NTB model [12]. The matrix elements of the Hamiltonian and overlap matrix elements for this model are derived as a function of the interatomic separation from the first principles [13]. This model allows for atomic structure relaxation, which is necessary for phonon modelling. The phonon dispersion of graphene is further derived in the adiabatic approximation by a perturbative approach within the NTB model [11]. The dynamical matrix is derived by expanding the energy of the crystal lattice of graphene, distorted by a phonon, in a power series of the atomic displacements up to second order. The obtained expansion contains terms with second-order variations of the matrix elements in the atomic displacements treated in first-order perturbation theory and terms with first-order variations of the matrix elements in the atomic displacements treated in second-

order perturbation theory. The perturbative approach has the advantage over the frozen-phonon one of avoiding the computationally expensive enlarging of the original cell in the calculations of forces on atoms and derivation of the dynamical matrix in a single step.

The absence of a gap in graphene reflects on its phonon dispersion. The presence of electronic states close to the Fermi energy around the two points K and K' of the Brillouin zone favors scattering of electrons by phonons between such states. The scattering is more effective for phonons with stronger electron-phonon coupling. This is indeed the case with the LO and TO phonons close to the Γ and K points, resulting in finite slopes of these branches, which is a signature of the Kohn anomaly in graphene [8, 11]. Another consequence of the strong electron-phonon coupling is the renormalization of the phonon frequency and linewidth and modification of the Kohn anomaly. The renormalization is described here by going beyond the adiabatic approximation and explicitly accounting for the dynamic effects [7].

Finally, we adopt the quantum-mechanical description of the Raman scattering process, in which the system of the electrons and phonons of the system, and photons of the electromagnetic radiation, and their interactions are considered [14].This description allows for the account of the finite electron and phonon lifetime due to scattering processes [15].

3 Results and Discussion

3.1 Adiabatic Approximation

The atomic structure of graphene was relaxed within the NTB model by use of a 600×600 Monkhorst-Pack mesh in the Brillouin zone until the residual forces on all atoms were reduced below 0.01 eV/Å. The phonon calculations were performed for the relaxed structure by use of the dynamical matrix. The phonon frequencies were obtained with accuracy of 1 cm^{-1}. The NTB model is known to overestimate the optical branches of graphene by about 11% [11]. This was corrected here by scaling of the phonon frequencies by a factor of 0.9 yielding a very good agreement with the available experimental data [10,16,17].

The calculated phonon dispersion of graphene along the high-symmetry directions ΓK, KM, and ΓM is shown in Figure 1. The phonon frequency of the TO branch close to the K point and, in partucular, the $A_1^{'}$-mode frequency, is difficult to measure experimentally [10]. The inelastic x-ray scattering data [10, 17] and Raman data [18] indicate that this mode should be close to the LO and LA branch crossing at the K point. The DFT calculations position it at least ≈ 100 cm^{-1} above this crossing [8, 17]. The accurate treatment of the electron correlations within the Green's function approach using the GW method position this mode by 14 cm^{-1} below the crossing [19]. The NTB model yields LO and LA

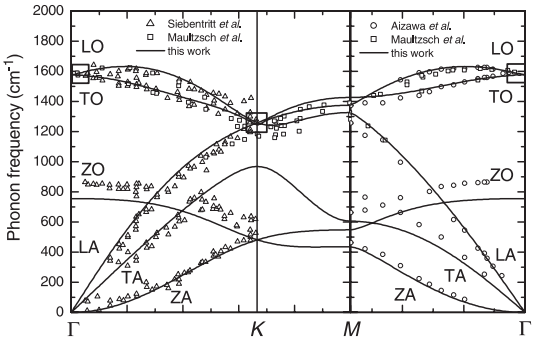

Figure 1. Calculated phonon dispersion of graphene along high-symmetry directions in the Brillouin zone in comparison with available experimental data. The phonon branches are marked with acronims of two letters with the following meaning: 'L' – longitudinal, 'T' - transverse, 'Z' – out-of-plane, 'O' – optical, and 'A' – acoustic. The regions with most significant changes of the branches due to dynamic effects are enclosed in rectangles.

branch crossing at 1267 cm^{-1} and the $A_1^{'}$-mode frequency to be by 32 cm^{-1} below the crossing [11], in fair agreement with the GW results. The NTB model has the advantage over the *ab-initio* models of inexpensive calculation of the phonon frequencies and eigenvectors at any point of the Brillouin zone and the consequent easy estimation of the changes of the phonon dispersion of graphene due to dynamic and doping effects. Because of the importance of the behaviour of the LO and TO branches around the Γ and K points, we present and discuss only results for these two branches along the ΓKM direction.

The obtained phonon dispersion of the LO and TO branches is linear in the wavevector at the Γ and K points, respectively, which is a signature of the Kohn anomaly [8] (Figure 1). The temperature dependence of the phonon dispersion was accounted for by smearing of the electron distribution close to the Fermi energy by use of the Fermi-Dirac distribution function. The calculations show that the temperature effect on the linearity of the two branches is negligable up to room temperature. For these reasons, here we report results only for $T = 300$ K.

The dynamical matrix is slowly converging with the number of $\mathbf{k}$ points, which can be explained with the zero gap of graphene at the K and K' points of the Brillouin zone [11]. This arises from terms of the dynamical matrix with energy denominator, vanishing at the two points. These terms can be written in the general form

$$\sum_{\mathbf{k}vc} \frac{M_{\mathbf{k}v,\mathbf{k}+\mathbf{q}c}}{E_{\mathbf{k}v} - E_{\mathbf{k}+\mathbf{q}c}}. \qquad (1)$$

Here, $E_{\mathbf{k}v}$ and $E_{\mathbf{k}+\mathbf{q}c}$ are the energies of the valence and conduction bands, respectively, depending on the electron wavevector $\mathbf{k}$ and the phonon wavevector

$\mathbf{q}$. The quantity $M_{\mathbf{k}v,\mathbf{k}+\mathbf{q}c}$ consists of first-order variations of the band-structure matrix elements in the atomic displacements. The summation is over the Brillouin zone and over the valence and conduction bands. The denominator of Eq. (1) vanishes for scattering of an electron by a zone-center phonon at the K or K' point or scattering of an electron by a K point phonon between the K and K' points. The sum Eq. (1) is actually convergent, which is readily seen if one considers linear electronic bands close to these two points and assumes a constant numerator. The sum can be transformed into an integral over $k \equiv |\mathbf{k}|$ between zero and some cut-off value with an area element $2\pi k dk$. The direct integration then yields a finite value.

The slopes of the LO and TO branches at the Γ and K points, β_Γ and β_K, respectively, can be directly associated with the electron-phonon coupling constants [8]. The previous DFT values [8] $\beta_\Gamma = 340$ cm^{-1} and $\beta_K = 973$ cm^{-1} have been corrected by recent GW data $\beta_\Gamma = 487$ cm^{-1} [20] and $\beta_K = 1504$ cm^{-1} [19]. The NTB model yields $\beta_\Gamma = 475$ cm^{-1} and $\beta_K = 1242$ cm^{-1}, in good agreement with the GW data, which justifies the use of the NTB model for simulation of processes and phenomena with important electron-phonon coupling.

3.2 Dynamic Effects

The phonon dispersion around the Γ and K points is largely modified due to strong electron-phonon interactions. The dynamic corrections to the phonon frequency, $\Delta\omega$, and the phonon linewidth, $\Delta\Gamma$, can be derived from the adiabatic dynamical matrix, by adding $\hbar\omega + i\delta$ to the energy denominator in Eq. (1), where ω is the adiabatic phonon frequency and δ is a small positive number [8, 21, 22]. Considering $\Delta\omega$ and $\Delta\Gamma$ to be small compared to ω, one can derive the expressions

$$\Delta\omega = \frac{1}{2\omega} Re\left\{\mathbf{e}^{+}\left[D\left(\hbar\omega + i\delta\right) - D\left(0\right)\right]\mathbf{e}\right\}. \tag{2}$$

$$\Delta\Gamma = \frac{\pi}{2\omega} Im\left[\mathbf{e}^{+} D\left(\hbar\omega + i\delta\right)\mathbf{e}\right]. \tag{3}$$

Here, $D\left(\hbar\omega + i\delta\right)$ is the corrected dynamical matrix, $D\left(0\right)$ is the adiabatic dynamical matrix and $\mathbf{e}$ is the phonon eigenvector.

The corrected high-frequency phonon dispersion in the vicinity of the Γ and K point, calculated by means of Eqs. (2) and (3), are shown in Figure 2. It is evident that while the G-mode and $A_1^{'}$-mode frequencies have zero dynamic corrections, large changes of the phonon dispersion are present for non-zero phonon wavevectors. The most important one is the appearence of a zero slope of the LO and TO branches at the two points in place of the finite one. In the vicinity of the Γ point, the LO and TO branches remain almost flat up to some phonon wavevector q_Γ (Figure 2, left), where the LO branch has a kink and the

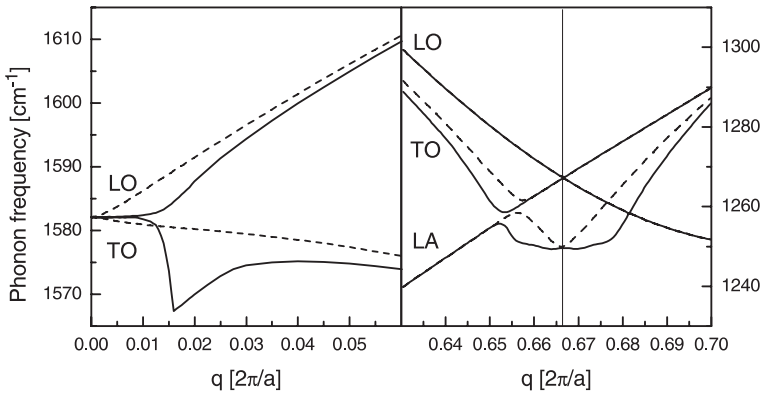

Figure 2. Calculated LO and TO branches close to the Γ point (left), and LO, TO, and LA branches close to the K point along the ΓKM direction (right). The curves in the adiabatic approximation are drawn in solid lines and those with dynamic corrections are drawn in dashed lines. The position of the K point is marked with a vertical line. Note the avoided crossing of the TO and LA branches at ≈ 0.65 splitting the TO branch into two parts.

TO branch reaches a minimum. Similarly, the TO branch at the K point has an almost flat region of size of $\sim 2q_K$, determined by some wavevector q_K relative to the K point (Figure 2, right). These features of the corrected phonon dispersion can be considered as signatures of the Kohn anomaly. For larger wavevectors both LO and TO branches tend to those obtained in the adiabatic approximation.

The corrected linewidth of the LO and TO phonons around the Γ and K point is shown in Figure 3. As seen in Figure 3, left, with the increase of the wavevector from the Γ point, the linewidth for the TO branch reaches a maximum at wavevector q_Γ and then decreases to zero, while the linewidth for the LO branch decreases monotonously to zero. The linewidth for the TO branch reaches a maximum at the K point and decreases rapidly away from it (Figure 3, right).

The behavior of $\Delta\omega$ and $\Delta\Gamma$ can be explained by arguments, similar to those, provided for metallic nanotubes [23]. In the latter study, the integration over the one-dimensional wavevector (see Eq. (1) with $\hbar\omega$ added to the denominator) is split into three regions: $(-\infty, -q_{\Gamma,K})$, $[-q_{\Gamma,K}, 0]$, and $(0, \infty)$, where $q_{\Gamma,K} \sim \hbar\omega_{\Gamma,K}/\beta_F$, β_F is the slope of the electronic bands at the Fermi energy and the indices Γ and K denote phonons in the vicinity of these two points. The wavevectors $q_{\Gamma,K}$ and 0 separate regions with back- and forward scattering of electrons. The different dependence of $\Delta\omega$ and $\Delta\Gamma$ on the wavevector for the LO and TO branches stems in the fact that the electron-phonon coupling in metallic nanotubes is nonzero only for back- and forward scattering of electrons from LO and TO phonons close to the Γ point, respectively, and for backscatter-

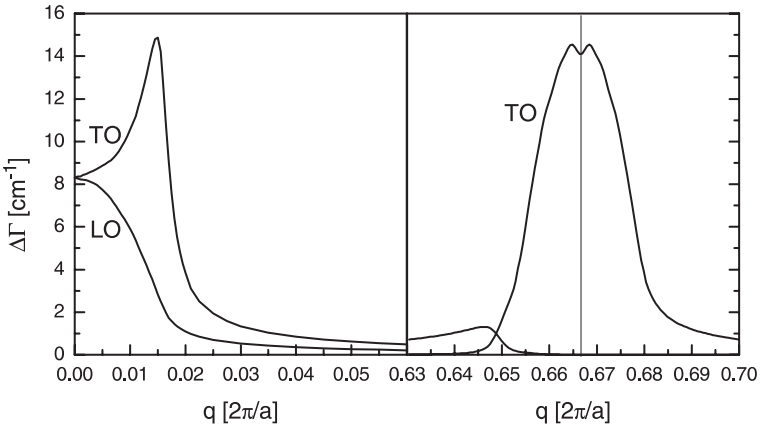

Figure 3. Calculated phonon linewidth $\Delta\Gamma$ for the LO and TO branches close to the Γ point (left), and for the TO branch close to the K point along the ΓKM direction (right). The position of the K point is marked with a vertical line. The two curves correspond to the two parts of the TO branch in Figure 2, right.

ing from TO phonons close to the K point. It has been proven analytically that this character of the electron scattering gives rise to a dip in the LO branch and a singularity in the TO branch at phonon wavevector q_Γ. From the same study, though not explicitly written, it follows also that the linewidth of the LO branch has a maximum at the Γ point and decreases away from it, and the linewidth of the TO branch has a maximum at q_Γ and decreases rapidly away from it. In graphene, due to the two-dimensionality of the structure, such analytical derivations are difficult to accomplish. However, qualitative conclusions can be drawn taking into account that the electron scattering from LO and TO phonons close to the Γ point is predominantly back- and forward scattering, respectively, and the scattering from TO phonons close to the K point is predominantly backscattering (see Eq. (6) in Ref. [8]). This result implies the existence of characteristic phonon wavevectors with length $q_{\Gamma,K}$ for graphene as well and similar behavior of the phonon dispersion and linewidth in both metallic nanotubes and graphene, as summarized in the previous two paragraphs.

In the NTB model, $\beta_F = 12.8$ eV for wavevector in units of $2\pi/a$, where a is the lattice parameter of graphene. This value of the slope corresponds to electron velocity at the Fermi energy $v_F = 8.0 \times 10^5$ m/s. For the G-mode $\omega_\Gamma = 0.196$ eV and $q_\Gamma = 0.0153$, and for the $A_1^{'}$-mode $\omega_K = 0.154$ eV and $q_K = 0.0120$. Therefore, the regions of importance of the dynamic effects are circles centered at the Γ and K points of size ≈ 50 times smaller than the size of the Brillouin zone of graphene. Outside these regions, the dynamic effects are negligible and the adiabatic approximation yields reasonable predictions for the phonon dispersion.

3.3 Doping Effects

The charge doping generally modifies the electronic structure of graphene. In the band approximation, the introduction of charges to the conduction bands or the removal of charges from the valence bands simply changes the band contribution of the total energy and the system relaxes to a state with a different lattice parameter. For doping levels of $\sim 10^{12}$ cm^{-2}, corresponding to Fermi energy shifts $E_F \sim 0.1$ eV, the variation of the lattice parameter is negligible (see also Ref. [7]). For these reasons, the calculations for doped graphene were performed for the relaxed structure at zero doping.

The charge doping of graphene produces an upshift of the phonon dispersion, the most affected being the LO and TO phonon branches close to the Γ and K points (Figure 4). The characteristic features, due to the dynamic correction, *e.g.*, the flat regions around these points, the kink of the LO branch, and the pronounced dip of the TO branch at q_Γ, tend to be gradually smeared out with the increase of the doping level. For $|E_F| = 0.3$ eV the flat region is still present but the dip is no longer noticeable. For the same doping, the frequencies of the G-mode and the $A_1^{'}$-mode become higher by 11 cm^{-1} and 32 cm^{-1}, respectively, compared to undoped graphene. With the increase of the phonon wavevector, these corrections become smaller and outside the regions of size q_Γ and q_K they are negligible. The doping effect on the phonon linewidth is illustrated in Figure 5. The increase of the doping level results in a decrease of the correction to the phonon linewidth. For $|E_F| = 0.3$ eV this correction is already below 1 cm^{-1}.

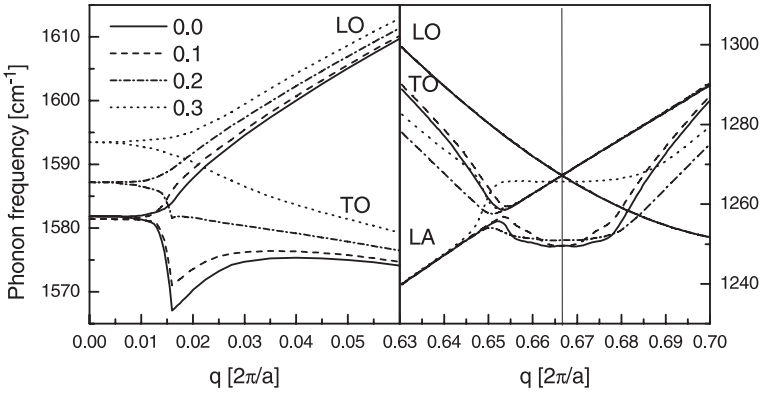

Figure 4. Calculated LO and TO branches close to the Γ point (left), and LO, TO, and LA branches close to the K point along the ΓKM direction (right) for four different Fermi energy shifts $E_F = 0.0$, 0.1, 0.2, and 0.3 eV. The position of the K point is marked with a vertical line.

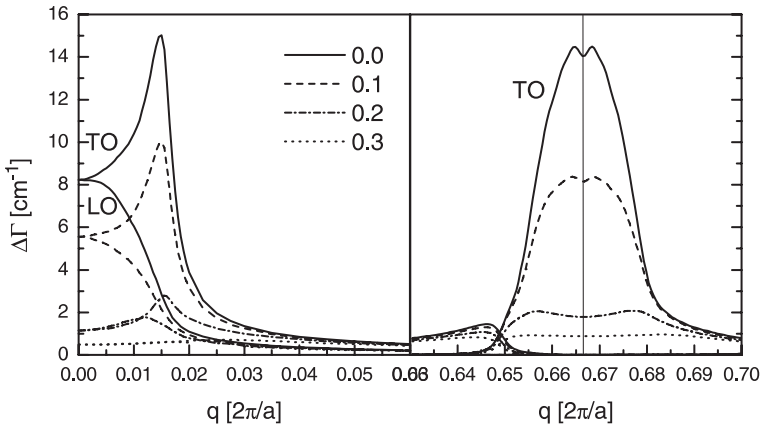

Figure 5. Calculated phonon linewidth $\Delta\Gamma$ for the LO and TO branches close to the Γ point (left) and for the TO branch close to the K point along the ΓKM direction (right) for four different Fermi energy shifts $E_F = 0.0$, 0.1, 0.2, and 0.3 eV. The position of the K point is marked with a vertical line.

Figure 6 shows that the frequencies of the G-mode and $A_1^{'}$-mode are almost constant for Fermi energy shift $|E_F|$ up to 0.1 eV and 0.08 eV, respectively, and increase quasi-linearly outside these regions. The calculated G-mode and $A_1^{'}$-mode linewidths (Figure 7) are significant for $|E_F|$ up to ≈ 0.1 eV but become small outside this region, decreasing steeply with the increase of the Fermi energy shift. The zero-doping linewidth has a maximum value of 8.3 cm^{-1} for the G-mode and 14.2 cm^{-1} for the $A_1^{'}$-mode. The former value agrees well with available experimental ones of 8 cm^{-1} [3] and 8.5 cm^{-1} [4].

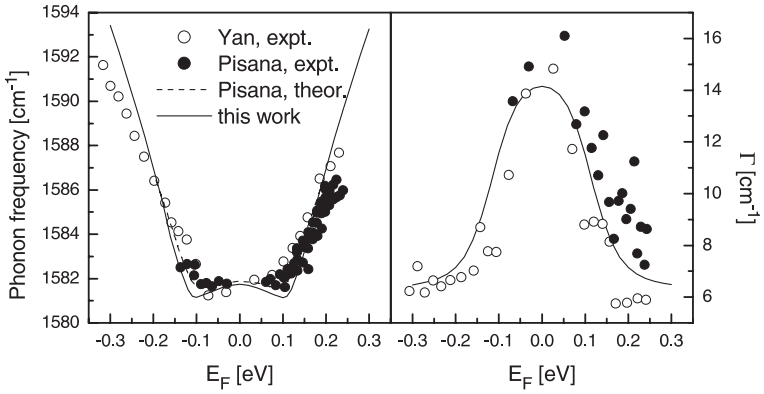

Figure 6. Left) Calculated G-mode frequency *vs.* Fermi energy shift E_F in comparison with experimental data and theoretical predictions. Right) Calculated A_1'-mode frequency *vs.* Fermi energy shift E_F.

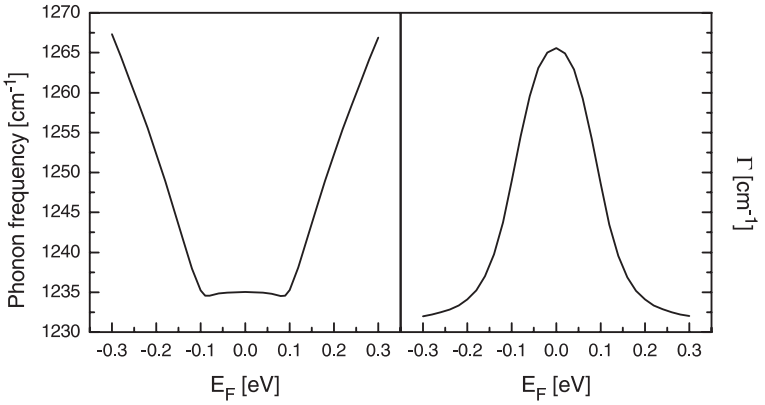

Figure 7. Left) Calculated phonon linewidth of the G-mode $\Gamma_0 + \Delta\Gamma$ *vs.* Fermi energy shift E_F in comparison with available experimental data. $\Gamma_0 = 6$ cm^{-1} is the contribution to the linewidth, which is not associated with electron-phonon coupling. Right) Calculated phonon linewidth of the A_1'-mode *vs.* Fermi energy shift E_F.

The dependence of the frequency and linewidth of the G-mode on the doping level can be explained with the effective phonon renormalization *via* electron-hole creation and annihilation. As it is seen from Eq. (1) with $\hbar\omega$ added to the denominator to account for dynamic effects, such processes can take place if occupied (empty) and empty (occupied) states are present in the valence and conduction bands, respectively, which satisfy the condition $E_{\mathbf{k}c} - E_{\mathbf{k}v} = \hbar\omega$. Such states exists for doping levels up to $|E_F| = \hbar\omega/2$. Thus, this value of E_F determines the crossover between the regime with strong and weak phonon renormalization. The behavior of $\Delta(\hbar\omega)$ and $\Delta\Gamma$ of the G-mode *vs.* E_F at $T = 0$ K can be described approximately by the formulas [3, 4]

$$\Delta(\hbar\omega) = \alpha\left\{|E_F| + \frac{\hbar\omega}{4}\ln\left|\frac{2\,|E_F| - \hbar\omega}{2\,|E_F| + \hbar\omega}\right|\right\}, \tag{4}$$

$$\Delta\Gamma = \begin{cases} \alpha\frac{\pi\hbar\omega}{4} & |E_F| \le \frac{\hbar\omega}{2} \\ 0 & |E_F| > \frac{\hbar\omega}{2} \end{cases}. \tag{5}$$

Here $\alpha = AD^2/2\pi\hbar\omega M v_F^2$, A is the unit cell area, D is the electron-phonon coupling constant, and M is the carbon atom mass. According to Eq. (4), $\Delta(\hbar\omega)$ has two logarithmic singularities at $|E_F| = \hbar\omega/2$ and linear asymptotic behavior for large $|E_F|$. Equation (5) predicts a finite linewidth correction for $|E_F| \le \hbar\omega/2$ and zero, otherwise. For finite temperatures, the logarithmic singularities are smeared out and the rectangular shape of the linewidth is smoothened, as can be observed from the obtained results in Figure 6. The frequency and linewidth of the $A_1^{'}$-mode are given by expressions, analogous to Eqs. (4) and (5).

The slope of the calculated frequency shift of G-mode *vs.* doping allows one to determine the electron-phonon coupling constant by means of the asymptotic formula [4]: $\Delta(\hbar\omega) = \alpha|E_F|$. Thus, we obtain $\alpha = 52$ cm^{-1}/eV and $D = 11.4$ eV/Å, in fair agreement with the experimental values of $12.6-14.1$ eV/Å [4] and to the theoretical one of 13.5 eV/Å, derived within the DFT [7]. The electron-phonon coupling D can be determined more precisely from the maximum of the phonon linewidth and the formula [4]: $\Delta\Gamma = AD^2/8Mv_F^2$. Our estimation for the coupling at the Γ point is $D = 11.2$ eV/Å. Previous NTB calculations of the electron-phonon coupling matrix elements of nanotubes yielded in the large-radius limit $D = 12.8$ eV/Å. However, since D determines the squared phonon frequencies, the scaling of the frequencies by 0.9 corresponds to scaling of D by $0.9^2 = 0.81$. Consequently, the scaled value of the latter matrix element should be ≈ 10.4 eV/Å, which is close to that, derived from the linewidth here. Similarly, for the electron-phonon coupling at the K point (Figure 7) we get $D = 14.7$ eV/Å, which corresponds well to the previous NTB value [9] of 18.1 eV/Å after downscaled the latter by a factor of 0.81.

3.4 Raman Intensity

Finally, we calculate the resonance Raman intensity of the G-mode with dynamic corrections as a function of the doping level for parallel scattering geometry [15]. The intensity was averaged over all possible orientations in space

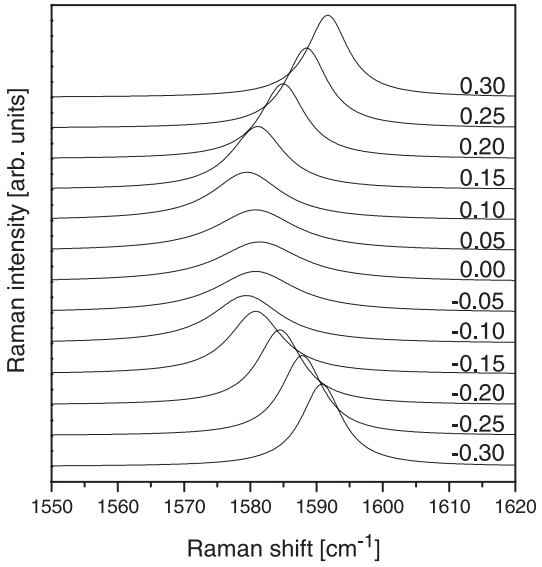

Figure 8. Calculated Raman spectra in the high-frequency region including the G-mode for different Fermi energy shifts E_F from -0.3 to 0.3 eV.

of the laser photon polarization for better correspondence with the common experimental setup. The effect of the finite phonon linewidth is accounted for by a Lorentzian broadening of the Raman line. The calculated Raman spectra of graphene, shown in Figure 8, exhibit an increasing blue-shift of the G-line position with the increase of the doping level, while the G-line peak value increases abruptly from an almost constant value to a larger one at $|E_F| \approx 0.1$ eV. This behavior is observed in the experimental Raman spectra [4].

4 Conclusions

We showed that the dynamic corrections have significant effect on the phonon dispersion of graphene in the vicinity of the Γ and K points and modify the adiabatic Kohn anomaly. We reproduce the *ab-initio* results for the G-mode frequency and predict the dynamic correction of the phonon dispersion, which is important for interpretation of the experimental data on double-resonance Raman scattering as well as for modeling of electron-phonon scattering processes in graphene. We also studied the doping dependence of the phonon dispersion close to the two special points, the major doping effect being the smearing out of the Kohn anomaly with the increase of the doping level.

Acknowledgments

V.N.P. was supported by NSF under grant DO 02-136/15.12.2008 (IRC-CoSiM).

References

[1] K. S. Novoselov, A. K. Geim, S. V. Morozov, D. Jiang, Y. Zhang, S. V. Dubonos, I. V. Grigorieva, A. A. Firsov (2004) *Science* **306** 666.

[2] C. Berger, Z. Song, X. Li, X. Wu, N. Brown, C. Naud, D. Mayou, T. Li, J. Hass, A. N. Marchenkov, E. H. Conrad, P. N. First, W. A. de Heer (2006) *Science* **312** 1191.

[3] S. Pisana, M. Lazzeri, C. Casiraghi, K. S. Novoselov, A. K. Geim, A. C. Ferrari, F. Mauri (2007) *Nature Materials* **6** 198.

[4] J. Yan, Y. Zhang, Ph. Kim, A. Pinczuk (2007) *Phys. Rev. Lett.* **98** 166802.

[5] X. Du, I. Skachko, A. Barker, E. Y. Andrei (2008) *Nature Nanotechnology* **3** 491.

[6] A. Das, B. Chakraborty, S. Piscanec, S. Pisana, A. K. Sood, A. C. Ferrari (2009) *Phys. Rev. B* **79** 155417.

[7] M. Lazzeri, F. Mauri (2006) *Phys. Rev. Lett.* **97** 266407.

[8] S. Piscanec, M. Lazzeri, F. Mauri, A. C. Ferrari, J. Robertson (2004) *Phys. Rev. Lett.* **93** 185503.

[9] V. N. Popov, Ph. Lambin (2006) *Phys. Rev. B* **74** 075415.

[10] M. Mohr, J. Maultzsch, E. Dobardžić, S. Reich, I. Milosević, M. Damnjanović, A. Bosak, M. Krisch, C. Thomsen (2007) *Phys. Rev. B* **76** 035439.

[11] V. N. Popov, Ph. Lambin (2006) *Phys. Rev. B* **73** 085407.
[12] V. N. Popov, L. Henrard (2004) *Phys. Rev. B* **70** 115407.
[13] D. Porezag, Th. Frauenheim, Th. Köhler, G. Seifert, R. Kaschner (1995) *Phys. Rev. B* **51** 12 947.
[14] R. M. Martin, L. Falicov (1975) in: *Topics of Applied Physics* **3**, ed. M. Cardona; Springer, Berlin.
[15] R. Loudon (1963) *Proc. Roy. Soc. (London)* **275** 218.
[16] S. Siebentritt, R. Pues, K.-H. Rieder, and A. M. Shikin (1997) *Phys. Rev. B* **55** 7927.
[17] J. Maultzsch, S. Reich, C. Thomsen, H. Requardt, P. Ordejón (2004) *Phys. Rev. Lett.* **92** 075501.
[18] L. M. Malard, D. L. Mafra, S. K. Doorn, M. A. Pimenta (2009) *Solid State Commun*. **149** 1136.
[19] A. Grüneis, J. Serrano, A. Bosak, M. Lazzeri, S. L. Molodtsov, L. Wirtz, C. Attaccalite, M. Krisch, A. Rubio, F. Mauri, T. Pichler (2009) *Phys. Rev. B* **80** 085423.
[20] M. Lazzeri, C. Attaccalite, L. Wirtz, F. Mauri (2008) Phys. Rev. B **78** 081406(R).
[21] H. Haken (1978) *Quantum field theory of solids: an introduction*; North-Holland, Amsterdam.
[22] W. E. Pickett, P. B. Allen (1977) *Phys. Rev. B* **16** 3127.
[23] S. Piscanec, M. Lazzeri, J. Robertson, A. C. Ferrari, F. Mauri (2007) *Phys. Rev. B* **75** 035427.
[24] C. M. Varma, W. Weber (1979) *Phys. Rev. B* **19** 6142.
[25] V. N. Popov, L. Henrard, Ph. Lambin (2005) *Phys. Rev. B* **72** 035436.